Calculation of the momentum distributions of positron annihilation radiation in Ge

1997 J. Phys.: Condens. Matter 9 8147

(http://iopscience.iop.org/0953-8984/9/38/018)

J. Phys.: Condens. Matter **9** (1997) 8147–8154. Printed in the UK PII: S0953-8984(97)79281-6

Calculation of the momentum distributions of positron annihilation radiation in Ge

W LiMing, B K Panda, S Fung and C D Beling

Department of Physics, The University of Hong Kong, Pokfulam Road, Hong Kong

Received 4 November 1996, in final form 12 June 1997

Abstract. One- and two-dimensional momentum distributions of positron annihilation radiation in Ge are calculated using the independent-particle model (IPM), the local density approximation (LDA) and the generalized gradient approximation (GGA). It is found that these three approximations are all capable of reproducing the main structures of the momentum distributions observed in the one- and two-dimensional angular correlation of positron annihilation radiation measurements. The positron annihilation rate is, however, found to be overestimated in the LDA in the low-momentum regime. While the GGA alone gives the correct total annihilation rate, it is found that the GGA is essentially just scaled with the LDA, and introduces no new momentum dependence to eliminate the overestimation of the LDA in the low-momentum regime.

1. Introduction

The technique of angular correlation of positron annihilation radiation (ACAR) has become a well established method for measuring the electron momentum distributions in solids, since the annihilation radiation carries information on the electron momenta [1, 2]. The three-dimensional electron momentum density may be reconstructed from the two-dimensional (2D) ACAR experimental data, giving an accurate picture of the electron momenta in solids [3]. A number of measurements on the electron momentum distribution in Ge [3–8] have been made in the past few decades. The general feature of the observed 2D momentum distribution of annihilation radiation in Ge can be summarized as follows.

(1) A deep and a shallow 'valley' appear in the [110] and [100] directions, respectively;
(2) there is a 'terrace' at around zero momentum;
(3) there exists a cut-off in the [110] direction, corresponding to the Jones zone surface; and
(4) the autocorrelation function, which is the Fourier transform of the momentum distribution, shows nodes which, in contrast to those observed in Compton profile (CP) measurements [10, 11], are slightly shifted from the exact lattice positions [3, 9].

Calculations based on the independent-particle model (IPM) approximation have reproduced the shape of positron annihilation radiation momentum distributions with some success [12–16]. This model does not, however, give correct total positron annihilation rates, as obtained by integrating the momentum density over the whole range of the momentum space. For example, we obtain an IPM positron lifetime in Ge of 1.24 ns, which is five times larger than the experimental value (228 ps) [17], indicating a significant error, which has long been realized to originate from the strong positron–electron correlation that enhances

0953-8984/97/388147+08$19.50

the effective electron density at the site of the positron [18]. Introduction of a positron–electron correlation potential and an annihilation rate enhancement factor, both of which are taken in the first approximation to depend only on the local electron density (the local density approximation (LDA)), gives much more reasonable positron lifetime values [19]. The LDA, however, slightly overestimates the positron annihilation rate in the low-momentum regime, thus giving rise to shorter positron lifetimes than the experimental values. Moreover, the LDA also overestimates the cohesive energy in electronic structure calculations, for reasons connected with the shape of the correlation hole close to the nucleus. In the recently developed generalized gradient approximation (GGA), the depth of the correlation hole is reduced, as a result of which the cohesive energy is decreased, giving good agreement with experiment [20]. More recently, Barbiellini *et al* proposed, in a positron–electron system, a GGA correction for the positron–electron correlation potential and enhancement factor, and this successfully reproduces the experimental positron lifetimes in various metals and semiconductors [21, 22].

Although it has long been recognized that electron–positron correlation has a relatively minor influence on the shape of the annihilation radiation momentum distribution [23], it remains the case that there is still some perturbation needing to be catered for correctly. It is thus a matter of significant interest to see how well the GGA scheme predicts the observed shape of the momentum distribution in comparison with the IPM and LDA approximations. Some differences between the IPM, LDA and GGA are indeed expected, since as pointed out by Stroud and Ehrenreich in their pioneering work [24] the anisotropies of the momentum distribution are enhanced by the anisotropy of the positron wave functions in solids, and the latter is expected to vary according to the strength of the positron–electron correlation potential. To address this issue, we have in the present study performed calculations of the momentum distribution of positron annihilation radiation in Ge using the IPM, LDA and GGA approximations. For calculating the electron states, use has been made of the empirical pseudopotential method. This approach was encouraged by the work of Jarlborg *et al* who discovered that the empirical pseudopotentials gave a better agreement with the experimental electronic structures than the first-principles calculations [25]. The potentials for the positron states include the positron–ion (point-core) interaction, the positron–valence-electron interaction, and in the case of the LDA and GGA calculations the respective correlation potential between the positron and the surrounding electrons. The GGA incorporates the corrections proposed by Barbiellini *et al* into the correlation potential and the enhancement factor [21, 22].

A brief review of the theory is given in section 2, results and discussions in section 3, and finally, some conclusions are given in section 4.

2. Theory

In a 2D ACAR experiment, the single integral of the momentum density, $\rho^{2\gamma}(\boldsymbol{p})$, along a certain direction (say, the z-axis) is measured; that is,

$$N(p_x, p_y) = \int \mathrm{d}p_z \; \rho^{2\gamma}(\boldsymbol{p}) \tag{1}$$

whereas in the long-slit (1D) ACAR experiment the observable is the double integral of the momentum density over a plane (say, the x–y plane), namely,

$$N(p_z) = \int\int \mathrm{d}p_x \; \mathrm{d}p_y \; \rho^{2\gamma}(\boldsymbol{p}). \tag{2}$$

In equations (1) and (2) the momentum density is defined such that $\rho^{2\gamma}(\boldsymbol{p})\ \mathrm{d}p_x\ \mathrm{d}p_y\ \mathrm{d}p_z$ is the partial rate of annihilation into the element $\mathrm{d}p_x\ \mathrm{d}p_y\ \mathrm{d}p_z$ of momentum space. With this definition, it is important to note that if experimental distributions $N(p_x, p_y)$ and $N(p_z)$ are to be compared with theoretical predictions, they must be normalized to give the total annihilation rate, λ_{tot}, thus:

$$\lambda_{tot} = \int \rho^{2\gamma}(\boldsymbol{p})\ \mathrm{d}\boldsymbol{p} = \int \mathrm{d}p_z\ N(p_z) = \int \mathrm{d}p_x\ \mathrm{d}p_y\ N(p_x, p_y). \tag{3}$$

The momentum density is given theoretically as follows [15]:

$$\rho^{2\gamma}(\boldsymbol{p}) = \pi r_0^2 c \frac{2}{\Omega} \sum_{n\boldsymbol{k}} \left| \int \mathrm{e}^{\mathrm{i}\boldsymbol{p}\cdot\boldsymbol{r}} \psi_+(\boldsymbol{r}) \psi_{n\boldsymbol{k}}(\boldsymbol{r}) \sqrt{\gamma(\boldsymbol{r})}\ \mathrm{d}\boldsymbol{r} \right|^2 \tag{4}$$

where $\psi_+(\boldsymbol{r})$ and $\psi_{n\boldsymbol{k}}(\boldsymbol{r})$ are the positron and electron wave functions, respectively, $\gamma(\boldsymbol{r})$ is the annihilation rate enhancement factor (for the IPM, $\gamma(\boldsymbol{r}) = 1$), and Ω is the unit-cell volume. Since in general there will be a δ-function in equation (4) after integration, it is always more convenient to calculate the momentum distributions from the inverse Fourier transform of the autocorrelation function, $B^{2\gamma}(\boldsymbol{r})$, which is defined as

$$B^{2\gamma}(\boldsymbol{r}) = \int \rho^{2\gamma}(\boldsymbol{p}) \mathrm{e}^{\mathrm{i}\boldsymbol{p}\cdot\boldsymbol{r}}\ \mathrm{d}\boldsymbol{p}. \tag{5}$$

It follows from equations (1) and (2) that the 1D and 2D momentum distributions can be obtained from $B^{2\gamma}(0, 0, z)$ and $B^{2\gamma}(x, y, 0)$, respectively. Moreover, the autocorrelation function also finds important application in the construction of the 3D electron momentum density from the 2D ACAR data [3]. Expanding now the electron and positron wave functions into plane waves, the autocorrelation function may be written as [15]

$$B^{2\gamma}(\boldsymbol{r}) = \pi r_0^2 c \frac{2}{\Omega} \sum_{n\boldsymbol{G}'\boldsymbol{k}} \left| \sum_{\boldsymbol{G}} C_n(\boldsymbol{G}, \boldsymbol{k}) D_{enh}(\boldsymbol{G}' - \boldsymbol{G}) \right|^2 \exp[\mathrm{i}(\boldsymbol{G}' + \boldsymbol{k}) \cdot \boldsymbol{r}] \tag{6}$$

where $C_n(\boldsymbol{G}, \boldsymbol{k})$ are the coefficients of the plane-wave expansion of the electron wave functions, and $D_{enh}(\boldsymbol{G})$ are the coefficients of the combined plane-wave expansion of the positron wave function together with the enhancement factor, i.e.

$$\psi_+(\boldsymbol{r})\sqrt{\gamma(\boldsymbol{r})} = \frac{1}{\sqrt{\Omega}} \sum_{\boldsymbol{G}} D_{enh}(\boldsymbol{G}) \exp(\mathrm{i}\boldsymbol{G} \cdot \boldsymbol{r}). \tag{7}$$

In the present work electron wave functions are obtained using the empirical pseudopotential method. The empirical pseudopotentials for Ge are taken as $V_3 = -0.23$, $V_8 = 0.01$, $V_{11} = 0.06$ Ryd. The wave functions are expanded into 181 plane waves. The special-k-point scheme (10 k-points) of Chadi and Cohen [26] is used in the calculation of the electron density. Since positron annihilation with core electrons has not been considered in equations (4) and (6), it follows that the theoretically derived $N(p_z)$ and $N(p_x, p_y)$ momentum distributions will indicate lower values than experiment (which indicates a few per cent of such annihilations). This, however, is not considered a serious omission in the present work, because such core annihilation predominantly affects only the high-momentum part of the distributions, and the concern is to focus on correctly describing the low-momentum regime.

The positron wave function is obtained by diagonalizing the Hamiltonian in reciprocal-lattice space, with the potential taken as

$$V_+(\boldsymbol{r}) = V_{ion}(\boldsymbol{r}) + V_{val}(\boldsymbol{r}) + V_{corr}(\boldsymbol{r}) \tag{8}$$

where the positron–ion potential, $V_{ion}(\boldsymbol{r})$, is treated in the point-core approximation, $V_{val}(\boldsymbol{r})$ is the Hartree potential due to the valence electrons, and $V_{corr}(\boldsymbol{r})$ is the electron–positron correlation potential. The LDA correlation potential, $V_{corr}^{LDA}(\boldsymbol{r})$, used in the present work is that of Boroński and Nieminen [19], and the LDA enhancement factor as parametrized in reference [22] is

$$\gamma^{LDA}(\boldsymbol{r}) = 1 + 1.23r_s - 0.0742r_s^2 + \frac{1}{6}r_s^3 \tag{9}$$

where $r_s = [3/(4\pi n_-)]^{1/3}$, n_- being the electron density. In the GGA, corrections are introduced into the LDA correlation potential and enhancement factor in the form [22]

$$V_{corr}^{GGA}(\boldsymbol{r}) = V_{corr}^{LDA}(\boldsymbol{r})\mathrm{e}^{-\alpha\epsilon(r)/3} \tag{10}$$

and

$$\gamma^{GGA}(\boldsymbol{r}) = 1 + (\gamma^{LDA}(\boldsymbol{r}) - 1)\mathrm{e}^{-\alpha\epsilon(r)} \tag{11}$$

where the empirical constant α has been set to be 0.22 [22] and the function $\epsilon(\boldsymbol{r})$, that caters for the effect of non-uniform electron density, is given by

$$\epsilon(\boldsymbol{r}) = |\nabla n_-(\boldsymbol{r})|^2/(n_-(\boldsymbol{r})q_{TF})^2 \tag{12}$$

where q_{TF} is the Thomas–Fermi screening length.

3. Results and discussion

The 1D momentum distributions of the positron annihilation radiation in Ge along the [100], [110] and [111] directions, as calculated from the IPM, LDA and GGA approximations, are shown in figures 1(a), 1(b), 1(c). The experimental data in this figure are from the work of Shulman *et al* [6] and have been normalized according to equation (3) so that the total area of the momentum distribution matches the total annihilation rate (1/228 ps) as observed in positron lifetime spectroscopy [17]. It is seen that in the low-momentum regime (up to 0.7 au) the present GGA calculations are in good agreement with the experimental data, displaying correctly features such as the 'ridge' at $q \approx 0.15$ au in the [110] direction and the flat top in the [100] direction. In the high-momentum regime the calculated momentum distributions are less than the experimental value, but this can be understood, at least in part, because no positron annihilation with core electrons has been taken into account in the present calculations.

Figure 1(b) also shows the cut-off in the [110] direction due to the Jones zone surface. The cut-off, however, is not so steep as the experimental curve. When the resolution function of the experiment is taken into account this discrepancy will become more serious. In the seventies, Fujiwara and Hyodo presented and commented on this discrepancy between the IPM calculation and their positron annihilation experiment carried out on Si [27]. It is noted that the present LDA and GGA calculations have not improved the prediction of the steepness of the cut-off.

Figure 1 shows, as expected, that the absolute magnitudes of the IPM results are much smaller and the LDA results significantly larger than the experimental curves. With regard to the momentum distribution shape, however, the three approximations, i.e. the IPM, LDA and GGA, give nearly the same predictions. This is seen clearly in figure 2 where the curves in the [110] direction have been normalized to the same area. It is seen that the different approximations give rise to nearly the same structure, except that the LDA and GGA give a slightly higher momentum distribution at $q \sim 0$. This invariance derives from the fact that the LDA and GGA enhancement factors have very little momentum dependence.

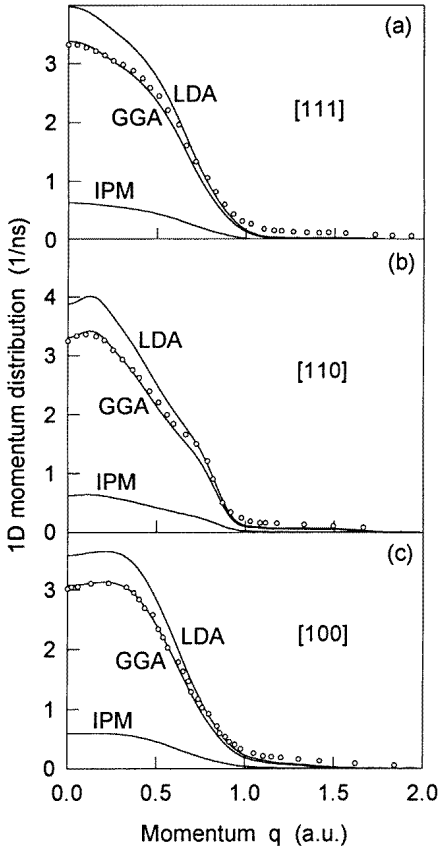

Figure 1. 1D momentum distributions in the directions of (a) [111], (b) [110] and (c) [100] calculated in the IPM, LDA and GGA approximations. The open circles show the experimental data of reference [6].

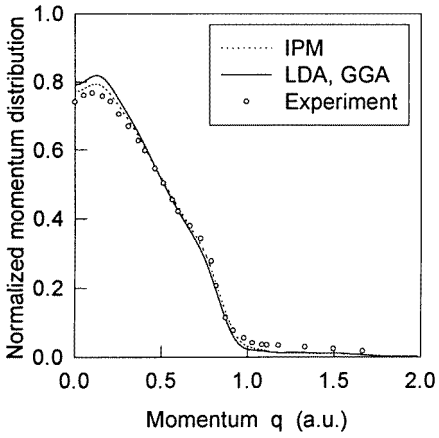

Figure 2. Normalized momentum distributions in the [110] direction. The lines show the results of the IPM, LDA and GGA calculations. The open circles show the experimental data of reference [6].

No noticeable difference is found between the LDA and GGA normalized distributions. Unfortunately, figure 2 shows that the LDA and GGA predictions for the shape of the momentum distribution are worse than those of the IPM. This unexpected result suggests that a better GGA-like approximation should contain a greater momentum dependence, in order to preferentially attenuate the LDA annihilation rate in the low-momentum region more than that in the high-momentum region. Identical results are found for the [100] and [111] directions. It can be seen that the momentum distribution is more sensitive to the details of the positron states in solids than the triply integrated quantity, the positron lifetime, since the positron lifetime in a number of metals and semiconductors, as pointed out by Barbiellini *et al* [21, 22], can be accurately reproduced in the GGA approximation.

In the Compton profile (CP) measurements, the zeros of the autocorrelation function, the Fourier inverted form factor, correspond exactly to the lattice positions. In the case of the positron annihilation radiation momentum distribution, however, the situation is similar but more complex owing to the necessity of convoluting the positron wave function and the enhancement factor, but to first order the zeros in the Fourier inverted distribution, the autocorrelation function, still correspond closely to the lattice positions, and thus this

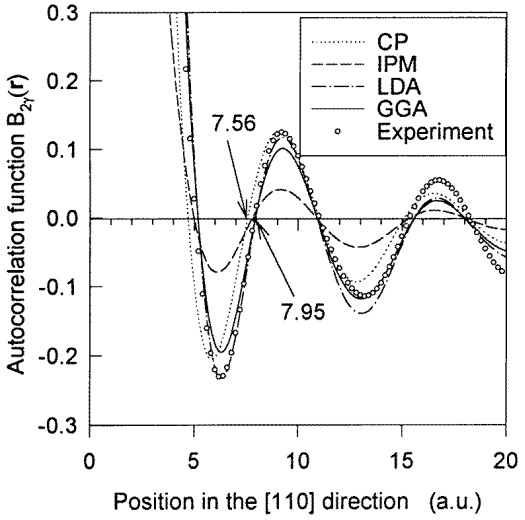

Figure 3. Autocorrelation functions in the [110] direction. The lines show the results of the CP, IPM, LDA and GGA calculations; the open circles show the Fourier transform of the experimental data of reference [6].

function still serves a useful role in allowing one to visualize the lattice environment of the site of annihilation [28]. It was found that, in the case of 1D or 2D ACAR measurements, the nodes of the autocorrelation shift to higher positions from the lattice sites [3, 6, 9]. The comparison between the present calculations and the experimental results of Shulman *et al* [6] are shown in figure 3. The first lattice point in the direction of [110] is at 7.56 au (4.0 Å) from the origin. The LDA and GGA calculations show a node at 7.95 au (4.2 Å), the exact experimental value, whereas the IPM calculation gives a lower value (7.75 au), that is not coincident with the experiment. The fourth node of the GGA calculation does not, however, agree with the experimental value, a feature which may be related to the discrepancy between the LDA/GGA calculations and experiment that is more dominant in the *low*-momentum regime.

In an anisotropy analysis, not only the isotropic core contribution but also the systematic errors in the experimental data may be eliminated. Therefore an anisotropy spectrum offers a more stringent test for the accuracy of a theoretical model. We have therefore presented the experimental and theoretical anisotropies between [100] and [110] directions, and between [100] and [111] directions in figures 4(a), 4(b). The experimental data are again from the work of Shulman *et al* [6]. It can be seen that the LDA and GGA calculations give stronger anisotropies, mainly in the low-momentum region, than the experimental data. This discrepancy is likely to be reduced when the experimental data are deconvoluted with the resolution function of the measurement. The IPM, however, certainly gives too weak an anisotropy at around zero momentum. This is as expected, since the IPM includes no enhanced annihilation for the low-momentum interstitial valence electrons that are preferentially sampled by the positron [13]. For comparison, the calculated CP anisotropies are also presented in figures 4(a), 4(b). They are much weaker than those of positron annihilation. While much of this weakening is undoubtedly due to the poor instrumental resolution of these early CP data, as with the IPM results, some will also derive from the absence of electron–positron correlation effects.

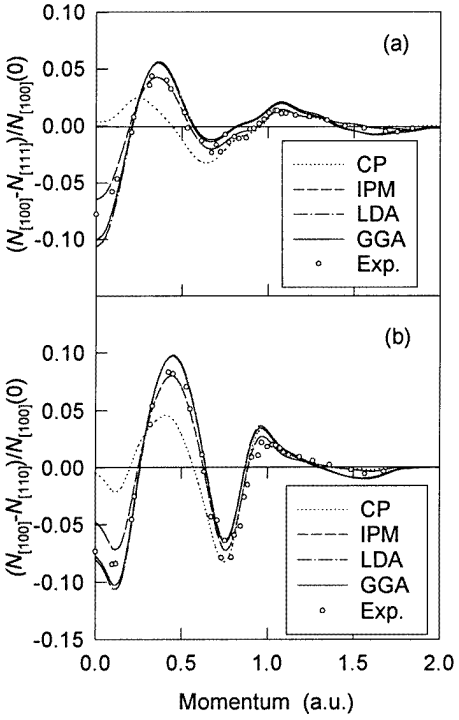

Figure 4. Anisotropies of the momentum distributions (a) between the [100] and [111] directions and (b) between the [100] and [110] directions. The open circles show the experimental data of reference [6].

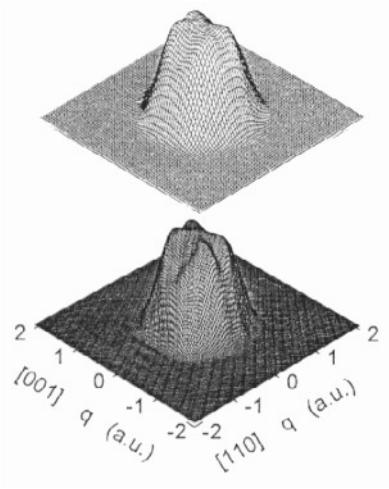

Figure 5. The 2D momentum distribution on the $(1\bar{1}0)$ plane (upper panel) from experiment [9] and (lower panel) from the GGA calculation of the present work.

We have calculated the 2D momentum distributions on the $(1\bar{1}0)$ plane in the IPM, LDA and GGA approximations. The result for the GGA is shown in figure 5. For comparison, we refer to the experimental data of West *et al* [8]. As can be seen in figure 5, a deep 'valley' extends up to the Jones zone surface in the [110] direction, a shallow 'valley' appears in the [100] direction, and a 'terrace' occurs at around zero momentum. These features are in good agreement with the experimental data, although the 'valleys' in the experimental data are smoother, a feature most probably caused by the limited resolution of the measurement. The present calculation is better than the LCAO calculation of Chiba and Akahane, which showed an obvious 'dip' at zero momentum and too short a 'valley' in the [110] direction [12]. In their calculation the positron wave function was assumed to be isotropic, leading to significant disagreement with experiment. Again, we find that the IPM and LDA results have generally similar features to the GGA calculation shown in figure 5. 2D anisotropies may provide more information on the positron states and the enhancement effect. For lack of the corresponding experimental data, the 2D anisotropies are not presented.

4. Conclusions

Calculations of the 1D and 2D momentum distributions of positron annihilation radiation in Ge have been performed, based on the IPM, LDA and GGA approximations. It has been found that the three approximations are more or less scaled with respect to each other.

The main structure, except for the enhanced annihilation rate effect, has been included in the IPM. Although only the GGA gives the correct total positron annihilation rate, it is found to have too weak a momentum dependence to eliminate the overestimation of the annihilation rate in the low-momentum region predicted by the LDA. In conclusion, we find that the GGA thus gives no noticeable improvement over the LDA as regards the shape of the annihilation radiation momentum distribution.

References

[1] Brandt W and Dupasquier A (ed) 1983 *Positron Solid State Physics* (Amsterdam: North-Holland)
[2] Puska M J and Nieminen R M 1994 *Rev. Mod. Phys.* **66** 841
[3] Kondo H, Cho Y-K, Kubota T, Kawano T, Watanabe K and Tanigawa S 1992 *J. Phys.: Condens. Matter* **4** 5911
[4] Erskine J C and McGervey J D 1966 *Phys. Rev.* **151** 615
[5] Reed W A and Eisenberger P 1972 *Phys. Rev.* B **6** 4596
[6] Shulman M A, Beardsley G M and Berko S 1975 *Appl. Phys.* **5** 367
[7] Arifov P U, Arutyunov N Yu, Trashchakov V Yu and Abdurasulev Z R 1983 *Sov. Phys.–Semicond.* **17** 1232
[8] West R N, Meyers J and Walters P A 1981 *J. Phys. E: Sci. Instrum.* **14** 478
[9] Berko S, Farmer W S and Sinclair F 1982 *Positron Annihilation* ed P G Coleman, S C Sharma and L M Diana (Amsterdam: North-Holland) p 319
[10] Pattison P and Schneider J R 1978 *Solid State Commun.* **28** 581
[11] Berko S, Farmer W S and Sinclair F 1982 *Positron Annihilation* ed W Brandt and A Dupasquier (Amsterdam: North-Holland) p 64
[12] Chiba T and Akahane T 1989 *Positron Annihilation* ed L Dorikens-Vanpraet, M Dorikens and D Segers (Singapore: World Scientific) p 674
[13] Saito M, Oshiyama A and Tanigawa S 1991 *Phys. Rev.* **19** 10 601
[14] Panda B K and Mahapatra D P 1993 *J. Phys.: Condens. Matter* **5** 3475
[15] Panda B K, Fung S and Beling C D 1996 *Phys. Rev.* B **53** 1251
[16] Aourag H, Belaidi A, Kobayashi T, West R N and Khelifa B 1989 *Phys. Status Solidi* b **155** 191
[17] Corbel C, Stucky M, Hautojarvi P, Saarinen K and Moser P 1988 *Phys. Rev.* B **38** 8192
[18] Kahana S 1963 *Phys. Rev.* **129** 1622
[19] Boroński E and Nieminen R M 1986 *Phys. Rev.* B **34** 3820
[20] Perdew J P, Chevary J A, Vosko S H, Jackson K A, Pederson M R, Singh D J and Fiolhais C 1992 *Phys. Rev.* B **46** 6671
[21] Barbiellini B, Puska M J, Torsti T and Nieminen R M 1995 *Phys. Rev.* B **51** 7341
[22] Barbiellini B, Puska M J, Korhonen T, Harju A, Torsti T and Nieminen R M 1996 *Phys. Rev.* B **53** 16 201
[23] Stewart A T 1957 *Can. J. Phys.* **35** 168
Carbotte J P 1967 *Phys. Rev.* **155** 197
[24] Stroud D and Ehrenreich H 1968 *Phys. Rev.* **171** 399
[25] Jarlborg T, Manuel A A, Peter M, Sanchez D, Singh A K, Stephan J-L and Walker E 1988 *Positron Annihilation* ed L Dorikens-Vanpraet, M Dorikens and D Segers (Singapore: World Scientific) p 266
[26] Chadi D J and Cohen M L 1973 *Phys. Rev.* B **8** 5747
[27] Fujiwara K and Hyodo T 1973 *J. Phys. Soc. Japan* **35** 1133
[28] Berko S 1983 *Positron Solid State Physics; Proc. 'Enrico Fermi' Int. School of Physics* vol 83, ed W Brandt and A Dupasquier (Amsterdam: North-Holland) p 64